Synthesis and Redox Properties of Amino Acid-Bridged Dinuclear Iron(III) Complexes

Keisuke Umakoshi,* Yasuhiro Tsuruma, Chang-Eon Oh,# Akira Takasawa, Hana Yasukawa, and Yoichi Sasaki*

Division of Chemistry, Graduate School of Science, Hokkaido University, Kita-ku, Sapporo 060-0810

(Received October 15, 1998)

A series of dinuclear iron(III) complexes with μ-O,O′-bridging amino acids (as zwitter ionic forms) have been prepared: $[Fe_2(\mu\text{-O})(\mu\text{-amino acid})(tpa)_2](ClO_4)_4$ (tpa = tris(2-pyridylmethyl)amine; amino acid = L-valine (**1**), L-proline (**2**), L-alanine (**3**), L-tyrosine (**4**), L-tryptophan (**5**), L-phenylalanine (**6**), L-alanyl-L-alanine (**7**)). Among them, **1**, **2**, and **7** were structurally characterized at 163 K. The non-equivalent ligating mode of the two tpa ligands is common to all the three complexes. The amino acid bridged complexes exhibit irreversible one electron reduction waves with splitting or accompanying shoulders. The bulk electrolysis of these complexes confirmed that the total number of electrons involved in the reduction is one; i.e. Fe_2(III, III) → Fe_2(II, III). Addition of acid or base leaves positive or negative components, respectively, of the splitting wave. This phenomenon was interpreted as a proton coupled electron transfer where the protonated and deprotonated amino acid bridged species are reduced at different potentials. Magnetic susceptibility measurements in the temperature range, 2—300 K, revealed antiferromagnetic coupling with $J = -116$, -129, -120, -120, and -129 cm^{-1} for **1**, **2**, **4**, **6**, and **7**, respectively ($H = -2JS_1 \cdot S_2$; $S_1 = S_2 = 5/2$).

Iron-containing proteins have attracted much attention owing to their ability of dioxygen transport and storage, activation of oxygen for insertion into a C–H bond, or a conduit for electron transfer.[1—6] Several dinuclear non-heme iron active sites and a number of their model complexes have been characterized structurally and spectroscopically,[7—24] and their functionalization[25—31] and the reaction with dioxygen[32—41] have been investigated. Recently, some O_2 coordinated diiron complexes have been characterized by X-ray structural analyses.[42—44]

Most of the model complexes involve anionic bridging ligands. In spite of the fact that in the enzyme diiron centers the bridging carboxylate groups are provided by the optically active amino acid residue of the surrounding proteins, virtually no model complex with bridging amino acids has been prepared. Recently, Tokii and co-workers reported the amino acid-bridged hexairon(III) complexes, $[Fe_6(O)_4(OH)_2(\text{amino acid})_4(phen)_8]^{9+}$ (amino acid = β-alanine or glycylglycine; phen = 1,10-phenanthroline).[45] We have reported amino acid-bridged diiron complexes, $[Fe_2(\mu\text{-O})(\mu\text{-amino acid})_2(tacn)_2]^{4+}$ (amino acid = L-valine and L-proline; tacn = 1,4,7-triazacyclononane), with a preliminary work on $[Fe_2(\mu\text{-O})(\mu\text{-amino acid})_2(tpa)_2]^{4+}$ (amino acid = L-valine, L-proline, and L-alanine; tpa = tris(2-pyridylmethyl)amine).[46] Amino acid-bridged trinuclear iron complexes have also been reported.[47,48] Oxo-bridged diiron complexes with bridging zwitter ionic amino acid provide the additional interesting point that proton-coupled redox reactions involving proton transfer from NH_3^+ group to the oxide bridge are possible, since the oxide bridge at the Fe_2(II, III) state could be strongly basic. In fact, it has been suggested that the protonation stabilizes the Fe_2(II, III) state in a protein environment.[10,49] Here we wish to report the further detailed study of synthesis and redox properties of a series of singly amino acid-bridged (in zwitter ionic form) diiron(III) complexes, $[Fe_2(\mu\text{-O})(\mu\text{-amino acid})(tpa)_2](ClO_4)_4$ (amino acid=L-valine, L-proline, L-alanine, L-tyrosine, L-tryptophan, L-phenylalanine, and L-alanyl-L-alanine).

Experimental

Synthetic Methods. The ligand tris(2-pyridylmethyl)amine (tpa) was prepared as described in the literature.[50] Acetonitrile was dried over calcium hydride and distilled under an argon atmosphere. Tetrabutylammonium hexafluorophosphate ($TBAPF_6$) was recrystallized twice from ethanol. All other commercially available reagents were used as purchased.

Caution! The perchlorate salts prepared in this study are all potentially explosive and should be handled in small portions with extreme care.

The seven $[Fe_2(\mu\text{-O})(\mu\text{-amino acid})(tpa)_2](ClO_4)_4$ complexes with different amino acids (μ-amino acid = L-valine (**1**), L-proline (**2**), L-alanine (**3**), L-tyrosine (**4**), L-tryptophan (**5**), L-phenylalanine (**6**), and L-alanyl-L-alanine (**7**)) were all synthesized in a similar manner. A typical preparation is as follows: A methanol solution (5 cm^3) of tpa (290 mg, 1 mmol) was added to a methanol solution (5 cm^3) of $Fe(ClO_4)_3 \cdot 10H_2O$ (534 mg, 1 mmol) with stirring. To the mixture was added an aqueous solution (5—10 cm^3) of amino acid (0.5 mmol) and the stirring was continued for 1 h. The re-

On leave from Department of Chemistry, Yengnam University, Gyongsam, Korea.

sulting brown precipitate was filtered, washed with methanol and ether, and dried in vacuo. Yield 70—85%. Elemental analyses and UV-vis data in CH_3CN (λ_{max}/nm (ϵ/dm^3 mol^{-1} cm^{-1})) of the new amino acid-bridged complexes are as follows. [$Fe_2(\mu$-O)(μ-L-valine)(tpa)$_2$](ClO_4)$_4$·CH_3CN·CH_3OH (**1**·CH_3CN·CH_3OH): Anal. Calcd for $C_{44}H_{54}Cl_4Fe_2N_{10}O_{20}$: C, 40.76; H, 4.19; N, 10.80; Cl, 10.94%. Found: C, 40.55; H, 4.11; N, 10.87; Cl, 11.00%. UV-vis 249 (27000), 328 (10400), 370 sh, 464 (1120), 485 (1060), 499 sh (980), 536 sh, 693 (147). [$Fe_2(\mu$-O)(μ-L-proline)(tpa)$_2$]-(ClO_4)$_4$ (**2**): Anal. Calcd for $C_{41}H_{45}Cl_4Fe_2N_9O_{19}$: C, 40.32; H, 3.71; N, 10.32; Cl, 11.61%. Found: C, 39.63; H, 3.79; N, 10.79; Cl, 11.16%. UV-vis 249 (28700), 330 (11600), 372 sh, 466 (1130), 487 (1090), 501 sh (1010), 537 sh, 696 (147). [$Fe_2(\mu$-O)(μ-L-alanine)(tpa)$_2$](ClO_4)$_4$ (**3**): Anal. Calcd for $C_{39}H_{47}Cl_4Fe_2N_9O_{21}$: C, 38.04; H, 3.85; N, 10.24; Cl, 11.52%. Found: C, 37.99; H, 3.94; N, 10.24; Cl, 11.57%. UV-vis 248 (29100), 329 (12000), 374 sh, 464 (1150), 485 (1090), 500 sh (1010), 534 sh, 695 (150). [$Fe_2(\mu$-O)(μ-L-tyrosine)(tpa)$_2$](ClO_4)$_4$ (**4**): Anal. Calcd for $C_{45}H_{47}Cl_4Fe_2N_9O_{20}$: C, 41.98; H, 3.68; N, 9.79; Cl, 11.02%. Found: C, 41.37; H, 3.89; N, 9.81; Cl, 11.33%. UV-vis 249 (30000), 330 (11900), 375 sh, 464 (1200), 484 (1140), 503 sh (1100), 695 (159). [$Fe_2(\mu$-O)(μ-L-tryptophan)(tpa)$_2$](ClO_4)$_4$ (**5**): Anal. Calcd for $C_{47}H_{48}Cl_4Fe_2N_{10}O_{19}$: C, 43.08; H, 3.69; N, 10.69; Cl, 10.82%. Found: C, 42.87; H, 3.79; N, 10.58; Cl, 10.83%. UV-vis 250 (32300); 329 (12200), 374 sh, 467 (1240), 483 (1210), 501 sh (1100), 693 (155). [$Fe_2(\mu$-O)(μ-L-phenylalanine)(tpa)$_2$]-(ClO_4)$_4$ (**6**): Anal. Calcd for $C_{45}H_{47}Cl_4Fe_2N_9O_{19}$: C, 42.51; H, 3.73; N, 9.92; Cl, 11.15%. Found: C, 41.85; H, 3.93; N, 9.90; Cl, 10.98%. UV-vis 249 (38400), 330 (16000), 372 sh, 466 (1060), 485 (1030), 503 sh (930), 699 (146). [$Fe_2(\mu$-O)(μ-L-alanyl-L-alanine)(tpa)$_2$](ClO_4)$_4$·$2CH_3CN$·C_4H_9OH (**7**·$2CH_3CN$·C_4H_9OH): Anal. Calcd for $C_{50}H_{64}Cl_4Fe_2N_{12}O_{21}$: C, 42.21; H, 4.53; N, 11.82; Cl, 9.97%. Found: C, 41.74; H, 4.55; N, 11.78; Cl, 9.95%. UV-vis 249 (28300), 331 (11300), 374 sh, 462 (1150), 490 (1020), 503 sh (920), 535 sh, 693 (153).

Crystallographic Studies. Crystals of **1** and **2** suitable for X-ray structural analyses were grown from the CH_3CN/MeOH solutions, while those of **7** were obtained from the CH_3CN/C_4H_9OH solution. The crystals were mounted on glass fibers and coated with a viscous perfluoroether. All data were collected on a MacScience MXC18 diffractometer using graphite-monochromated Mo $K\alpha$ (λ = 0.71073 Å) radiation at 163 K. Each unit cell parameter was obtained by least-squares refinement of 26 reflections ($30 \leq 2\theta \leq 35°$). The intensities of three standard reflections for each compound, monitored every 150 reflections, showed no appreciable decay during the data collection. All data were corrected for Lorentz and polarization effects. No absorption correction was made for all the three compounds.

The crystal structures were solved by direct method (SIR92)[51] for **1**·CH_3CN·CH_3OH and **2**·$2CH_3CN$·H_2O. The positional and thermal parameters of non-H atoms were refined anisotropically by the full-matrix least-squares method. The minimized function was $\Sigma w(|F_o| - |F_c|)^2$, where $w^{-1} = \sigma^2(|F_o|) + 0.0001|F_o|^2$. H atoms were included at calculated positions with fixed displacement parameters (1.3 times the displacement parameters of the host atom). In the final cycle of the refinement, parameter shifts were less than 0.1σ. No correction was made for secondary extinction.

The crystal structure of **7**·$2CH_3CN$·C_4H_9OH was also solved by direct method (SIR92).[51] The positional and thermal parameters of non-H atoms were refined anisotropically by the full-matrix least-squares method, except for those of O and Cl(4) atoms of ClO_4^- ions and those of CH_3CN and C_4H_9OH molecules. The Cl(4)–O(41), Cl(4)–O(42), Cl(4)–O(43), and Cl(4)–O(44) distances were fixed at 1.419 Å, which is the average Cl–O distance of the rest of perchlorate ions. We could not succeed to assign the O atom in C_4H_9OH molecule, thus all atoms in this molecule were refined as carbon. The minimized function was $\Sigma w(|F_o| - |F_c|)^2$, where $w^{-1} = \sigma^2(|F_o|) + 0.0001|F_o|^2$. No attempt was made to locate hydrogen atoms because of the low quality of intensity data. In the final cycle of the refinement, parameter shifts were less than 0.12σ. No correction was made for secondary extinction.

All calculations were performed using Crystan[52] and Bond.[53] The absolute configuration of the molecule for each compound was confirmed by the chirality of the bridging amino acid. Further crystallographic data are given in Table 1. Listings of selected bond distances and angles are summarized in Table 2. Tables of atomic coordinates and thermal parameters, full lists of bond lengths and bond angles, and tables of calculated and observed structure factors are deposited as Document No. 72011 at the Office of the Editor of Bull. Chem. Soc. Jpn.

Electrochemical Measurements. Cyclic voltammetry was performed with a BAS CV-50W Voltammetric Analyzer. The working and the counter electrodes were a glassy-carbon disk and a platinum wire, respectively. Cyclic voltammograms were recorded at a scan rate of 50 mV s^{-1}. The sample solutions (ca. 1.0 mmol dm^{-3}) in 0.1 mol dm^{-3} $TBAPF_6$–acetonitrile were deoxygenated with a stream of argon. The reference electrode was Ag/AgCl and the half-wave potential of Fc^+/Fc ($E_{1/2}(Fc^{+/0})$ vs. Ag/AgCl) was +0.430 V.

Controlled-potential coulometry was carried out in 0.1 mol dm^{-3} $TBAPF_6$–acetonitrile with a standard H-type cell with a Hokuto HA-310 potentiostat and a Hokuto HF-201 coulometer. The working electrode was made of platinum gauze, and the working compartment was separated from the counter compartment by a sintered-glass disk.

Magnetic Measurements. Magnetic susceptibility data were collected in the temperature range 2.0—300 K and in applied 10 kG field with the use of a Quantum Design Model MPMS SQUID magnetometer. Powdered samples were contained in the small half of a gelatin capsule. A phenolic guide (clear soda straw) was used to house the sample holder and was fixed to the end of the magnetometer drive rod. $[Cr(NH_3)_6](NO_3)_3$ was employed as dual magnetometer calibrant. Pascal's constants were used to determinate the constituent atom diamagnetism.

Other Measurements. The ^{1}H NMR spectra were obtained at 270 MHz with a JEOL JNM-EX270 spectrometer. ^{1}H chemical shifts were measured relative to the methyl resonance of TMS. UV-visible spectra were recorded on a Hitachi U3410 spectrophotometer at 20 °C. IR spectra were recorded on a Hitachi 270-50 infrared spectrophotometer.

Results and Discussion

Preparation of amino acid-bridged (μ-oxo)diiron(III) complexes of tris(2-pyridylmethyl)amine (tpa), [$Fe_2(\mu$-O)(μ-amino acid)(tpa)$_2$](ClO_4)$_4$, was straightforward. It should be stressed that even a dipeptide ligand, L-alanyl-L-alanine, can bridge two ferric ions by the terminal calboxyl group.

Que and co-workers have prepared a series of (μ-oxo)-diiron(III) complexes of tpa, [$Fe_2(\mu$-O)(tpa)$_2$(L)](ClO_4)$_n$, with negatively charged bridging ligands such as carboxylates, carbonate, maleate, diphenylphosphate, and some other related ligands.[23] Analogous diiron complexes with bridging neutral amino acids (zwitter ionic form) have not been pre-

Table 1. Crystallographic Data for $[Fe_2(\mu\text{-O})(\mu\text{-L-valine})(tpa)_2](ClO_4)_4\cdot CH_3CN\cdot CH_3OH$ (**1**·$CH_3CN\cdot CH_3OH$), $[Fe_2(\mu\text{-O})(\mu\text{-L-proline})(tpa)_2](ClO_4)_4\cdot 2CH_3CN\cdot H_2O$ (**2**·$2CH_3CN\cdot H_2O$) and $[Fe_2(\mu\text{-O})(\mu\text{-L-alanyl-L-alanine})(tpa)_2](ClO_4)_4\cdot 2CH_3CN\cdot C_4H_9OH$ (**7**·$2CH_3CN\cdot C_4H_9OH$)

	1·$CH_3CN\cdot CH_3OH$	**2**·$2CH_3CN\cdot H_2O$	**7**·$2CH_3CN\cdot C_4H_9OH$
Formula	$C_{44}H_{54}Cl_4Fe_2N_{10}O_{20}$	$C_{45}H_{53}Cl_4Fe_2N_{11}O_{20}$	$C_{50}H_{64}Cl_4Fe_2N_{12}O_{21}$
Cryst. system	Monoclinic	Monoclinic	Monoclinic
Space group	$P2_1$	$P2_1$	$P2_1$
a/Å	11.917(4)	11.899(3)	12.340(3)
b/Å	19.986(9)	19.784(4)	23.134(5)
c/Å	11.486(4)	11.667(3)	11.738(2)
β/deg	95.40(3)	93.31(2)	106.11(2)
V/Å^3	2723(2)	2742(1)	3219(1)
Z	2	2	2
T/°C	−110	−110	−110
d_{calcd}/(g cm^{-3})	1.58	1.60	1.47
Cryst size/mm	0.40 × 0.40 × 0.10	0.50 × 0.45 × 0.20	0.68 × 0.35 × 0.20
Scan mode	ω–2θ	ω–2θ	ω–2θ
Scan speed/(deg min^{-1})	8	8	8
$2\theta_{max}$/deg	55.0	55.0	55.0
μ(Mo $K\alpha$)/cm^{-1}	8.11	8.07	6.94
No. of unique rflns.	6210	6296	7151
No. of obsd rflns.	6015, $I > 2\sigma(I)$	6108, $I > 2\sigma(I)$	5925, $I > 3\sigma(I)$
R[a)]	0.047	0.042	0.085
R_w[b)]	0.056	0.049	0.090
GOF[c)]	2.03	1.76	4.01

a) $R = \Sigma||F_o| - |F_c||/\Sigma|F_o|$. b) $R_w = [\Sigma w(|F_o| - |F_c|)^2/\Sigma w|F_o|^2]^{1/2}$; $w^{-1} = \sigma^2(|F_o|) + 0.001|F_o|^2$ for **1**·$CH_3CN\cdot CH_3OH$ and **2**·$2CH_3CN\cdot H_2O$; $w^{-1} = \sigma^2(|F_o|)+0.0001|F_o|^2$ for **7**·$2CH_3CN\cdot C_4H_9OH$. c) The goodness of fit is defined as $[w(|F_o| - |F_c|)^2/(n_o - n_v)]^{1/2}$, where n_o and n_v denotes the numbers of data and variables, respectively.

pared previously. UV-vis spectra of the amino acid-bridged species are very similar to each other and also similar to those of the acetate-bridged complex.[23] The ^{1}H NMR spectra of **1**—**7** in CD_3CN show broad signals in the range from 0 to ca. 40 ppm, which are similar in pattern to the spectrum of $[Fe_2(\mu\text{-O})(\mu\text{-OAc})(tpa)_2]^{3+}$.[22] The magnetic properties of $[Fe_2(\mu\text{-O})(\mu\text{-amino acid})(tpa)_2](ClO_4)_4$ are also similar to that of $[Fe_2(\mu\text{-O})(\mu\text{-OAc})(tpa)_2]^{3+}$ (Table 3).[23]

Structure. X-Ray structural analyses have been conducted on complexes **1**, **2**, and **7** at 163 K. Figures 1, 2, and 3 show the ORTEP drawings of the three complex cations in **1**, **2**, and **7**, respectively. Selected bond lengths and angles are summarized in Table 2. These three structures are very similar to each other and also to that of the acetate bridged dimer, $[Fe_2(\mu\text{-O})(\mu\text{-OAc})(tpa)_2]^{3+}$.[22] Among these structural analyses, the structure of **7** is particularly noteworthy as a peptide like L-alanyl-L-alanine also bridges Fe–O–Fe moiety by the terminal carboxyl group. The two tpa ligands in each of **1**, **2**, and **7** have different orientations. The tpa ligand associated with Fe1 contains a pyridine ring *trans* to the oxo bridge, while the tpa ligand associated with Fe2 has the tertiary amine *trans* to the oxo bridge. As a consequence, the Fe1–N11 bond *trans* to the oxo bridge (2.20—2.21 Å) is significantly longer than the other five Fe–N_{py} bonds (2.11—2.16 Å). By comparing the Fe–N distances *trans* to the oxo bridge, we see that the Fe1–N11 (Fe–N_{py}) distance (2.20—2.21 Å) is slightly shorter than the Fe2–N2 (Fe–N_{amine}) distances (2.22—2.24 Å), which is in contrast to the fact that the Fe1–O1 bond (1.81—1.82 Å; *trans* to the Fe1–N11) is longer than the Fe2–O1 bond (1.77—1.78 Å; *trans* to the Fe2–N2).

The Fe1···Fe2 distance in **1** (3.305(2) Å), **2** (3.274(1) Å) and **7** (3.243(2) Å) decreases as the Fe1–O1–Fe2 angle decreases. However, as previously mentioned,[23] there also does not appear to be any correlation between antiferromagnetic coupling constant J and the Fe–O–Fe bridge angle in these complexes (Table 3). The lack of a correlation between J and the Fe–O–Fe angle in the tpa series was due to the rather small change in the structural parameters along the series, which obscures any appreciable trend in the J values if one existed.

Redox Properties. The amino acid-bridged diiron(III) complexes, $[Fe_2(\mu\text{-O})(\mu\text{-amino acid})(tpa)_2](ClO_4)_4$, show a splitting reduction wave at around 0 V vs. Ag/AgCl in CH_3CN. Reduction potentials (E^1_{pc} and E^2_{pc}) of each component (**I** and **II**, respectively) of the splitting wave of $[Fe_2(\mu\text{-O})(\mu\text{-amino acid})(tpa)_2](ClO_4)_4$ (**1**—**7**) are listed in Table 4. Figure 4 (a, top two) shows the cyclic voltammograms of **4** and **7**. A small reoxidation wave (**III**) coupled with the more negative peak (**II**) of the splitting reduction wave was observed. Thus the coupled wave (**II/III**) is regarded as a reversible or quasi-reversible process. An additional oxidation wave (**IV**) was observed at +0.45 V.

When an equimolar amount of *p*-toluenesulfonic acid or triethylamine was added to the solutions of **4** and **7**, the first reduction peak or the second one, respectively, gain increased current at the expense of the other peak. In the presence of *p*-toluenesulfonic acid, the amino acid bridged complexes are

Table 2. Selected Bond Lengths (Å) and Angles (deg) for $[Fe_2(\mu\text{-}O)(\mu\text{-}L\text{-valine})(tpa)_2](ClO_4)_4 \cdot CH_3CN \cdot CH_3OH$ (**1**·$CH_3CN \cdot CH_3OH$), $[Fe_2(\mu\text{-}O)(\mu\text{-}L\text{-proline})(tpa)_2](ClO_4)_4 \cdot 2CH_3CN \cdot H_2O$ (**2**·$2CH_3CN \cdot H_2O$), and $[Fe_2(\mu\text{-}O)(\mu\text{-}L\text{-alanyl-}L\text{-alanine})(tpa)_2](ClO_4)_4 \cdot 2CH_3CN \cdot C_4H_9OH$ (**7**·$2CH_3CN \cdot C_4H_9OH$)

	1·$CH_3CN \cdot CH_3OH$	**2**·$2CH_3CN \cdot H_2O$	**7**·$2CH_3CN \cdot C_4H_9OH$
Fe(1)···Fe(2)	3.305(2)	3.2742(7)	3.243(2)
Fe(1)–O(1)	1.812(3)	1.809(3)	1.818(7)
Fe(1)–O(3)	1.999(6)	2.002(3)	1.987(10)
Fe(1)–N(1)	2.195(6)	2.174(4)	2.176(10)
Fe(1)–N(11)	2.197(4)	2.210(4)	2.201(8)
Fe(1)–N(21)	2.134(4)	2.135(4)	2.148(14)
Fe(1)–N(31)	2.133(5)	2.143(4)	2.162(12)
Fe(2)–O(1)	1.784(4)	1.776(3)	1.773(6)
Fe(2)–O(2)	2.083(3)	2.096(3)	2.027(7)
Fe(2)–N(2)	2.243(4)	2.226(4)	2.222(8)
Fe(2)–N(41)	2.114(4)	2.122(4)	2.144(9)
Fe(2)–N(51)	2.119(4)	2.144(4)	2.121(9)
Fe(2)–N(61)	2.107(4)	2.112(4)	2.148(9)
Fe(1)–O(1)–Fe(2)	133.6(3)	131.9(2)	129.1(4)
O(1)–Fe(1)–O(3)	98.6(2)	100.5(2)	100.5(3)
O(1)–Fe(1)–N(1)	98.3(2)	96.1(2)	97.2(5)
O(1)–Fe(1)–N(11)	175.2(3)	172.0(2)	175.2(6)
O(1)–Fe(1)–N(21)	98.1(2)	94.0(2)	91.1(5)
O(1)–Fe(1)–N(31)	93.7(2)	94.7(2)	97.7(4)
O(3)–Fe(1)–N(1)	162.8(2)	162.9(2)	162.3(4)
O(3)–Fe(1)–N(11)	85.2(2)	85.9(2)	84.0(4)
O(3)–Fe(1)–N(21)	98.0(2)	104.6(2)	102.5(4)
O(3)–Fe(1)–N(31)	104.8(2)	97.6(2)	99.3(6)
N(1)–Fe(1)–N(11)	78.0(2)	78.0(2)	78.4(3)
N(1)–Fe(1)–N(21)	76.7(2)	78.2(2)	76.6(5)
N(1)–Fe(1)–N(31)	77.0(2)	76.7(2)	78.7(4)
N(11)–Fe(1)–N(21)	84.2(2)	79.6(2)	86.4(4)
N(11)–Fe(1)–N(31)	82.4(2)	89.2(2)	83.0(4)
N(21)–Fe(1)–O(31)	152.4(3)	154.2(2)	154.5(4)
O(1)–Fe(2)–O(2)	98.0(2)	98.0(2)	99.4(3)
O(1)–Fe(2)–N(2)	175.2(2)	178.2(2)	177.5(4)
O(1)–Fe(2)–N(41)	106.8(2)	103.5(2)	101.9(4)
O(1)–Fe(2)–N(51)	97.7(2)	100.2(2)	98.9(3)
O(1)–Fe(2)–N(61)	100.6(2)	103.0(2)	106.3(4)
O(2)–Fe(2)–N(2)	85.8(2)	83.3(2)	81.7(3)
O(2)–Fe(2)–N(41)	84.4(2)	88.1(2)	92.2(4)
O(2)–Fe(2)–N(51)	163.9(2)	161.5(2)	161.0(3)
O(2)–Fe(2)–N(61)	91.8(2)	90.2(2)	85.4(3)
N(2)–Fe(2)–N(41)	76.4(2)	77.7(2)	75.7(4)
N(2)–Fe(2)–N(51)	78.7(2)	78.6(2)	80.3(3)
N(2)–Fe(2)–N(61)	76.2(2)	75.7(2)	76.1(4)
N(41)–Fe(2)–N(51)	88.0(2)	84.4(2)	89.3(4)
N(41)–Fe(2)–N(61)	152.6(2)	153.3(2)	151.7(4)
N(51)–Fe(2)–N(61)	88.4(2)	89.0(2)	84.4(4)

reduced at more positive potential corresponding to wave **I** and wave **II** nearly disappears. Several features appear at more positive potentials than **I**, and also at reoxidation regions, indicating that some side reactions, possibly acid-assisted decomposition, take place. Thus the cyclic voltammograms in the presence of acid are not appropriate for detailed discussion. In the presence of triethylamine, on the other hand, the main reoxidation wave appeared at the position of wave **III** in the case of the complex **7** and at that of wave **IV** for the complex **4**. The peak height of reoxidation wave **IV** increases with concomitant decrease in wave **III** in the order of **7**, **2**, **3**, **5**, **6**, **1**, and **4**. Thus the relative current intensities of waves **III** and **IV** depend significantly on the kind of the bridging amino acid.

Controlled-potential coulometry for **4** and **7** at −0.4 V gave an overall electron stoichiometry of 0.90±0.05 e/Fe_2 for the splitting reduction wave.[54] Thus the one-electron reduction process is splitting. Such splitting was not observed for the acetate-bridged complex, $[Fe_2(\mu\text{-}O)(\mu\text{-}OAc)(tpa)_2]^{3+}$, where a simple reversible Fe_2(II, III)/(III, III) wave was observed in acetonitrile.[24]

These observations can be interpreted as follows (Scheme 1). At the first reduction potential (E^1_{pc}, **I**), the μ-oxo Fe_2(III, III) complexes with the zwitter ionic amino acid,

Table 3. Structural Data and Magnetic Properties of $[Fe_2(\mu\text{-}O)(L)(tpa)_2](ClO_4)_n$

	L = L-valine (**1**)[a]	L = L-proline (**2**)[a]	L = L-tyrosine (**4**)[a]	L = L-phenylalanine (**6**)[a]	L = L-alanyl-L-alanine (**7**)[a]	L = OAc[b]	L = OBz[b]
				Structural data			
Fe1···Fe2 (Å)	3.305(2)	3.2742(7)	—	—	3.243(2)	3.243(1)	3.241(1)
Fe1–O1 (Å)	1.812(3)	1.809(3)	—	—	1.818(7)	1.799(4)	1.808(3)
Fe2–O1 (Å)	1.784(4)	1.776(3)	—	—	1.773(6)	1.790(3)	1.774(3)
Fe1–O1–Fe2 (deg)	133.6(3)	131.9(2)	—	—	129.1(4)	129.2(2)	129.7(3)
				Magnetic properties			
$-J$ (cm^{-1})[c]	116(1)	129(1)	120(1)	120(1)	129(1)	114.3	118.6
μ_{eff} (B.M.)[d]	2.45	2.28	2.41	2.42	2.25		

a) $n = 4$, b) $n = 3$; Refs. 22 and 23, c) $H = -2JS_1 \cdot S_2$, $S = 5/2$, d) Values at 300 K.

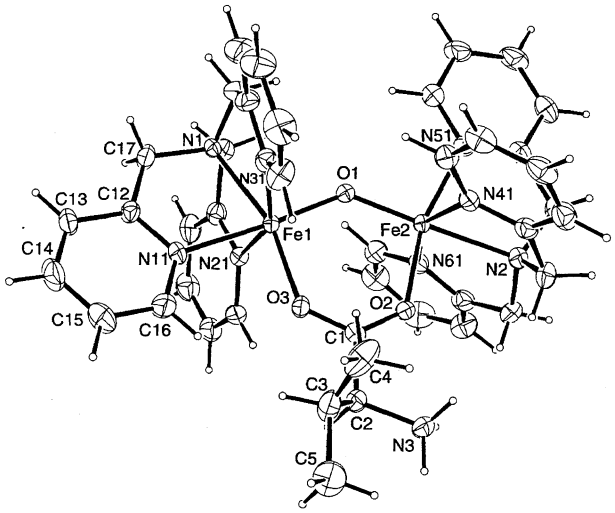

Fig. 1. ORTEP drawing of the complex cation in $[Fe_2(\mu\text{-}O)(\mu\text{-L-valine})(tpa)_2](ClO_4)_4 \cdot CH_3CN \cdot CH_3OH$ with the atomic numbering scheme showing 50% probability thermal ellipsoids.

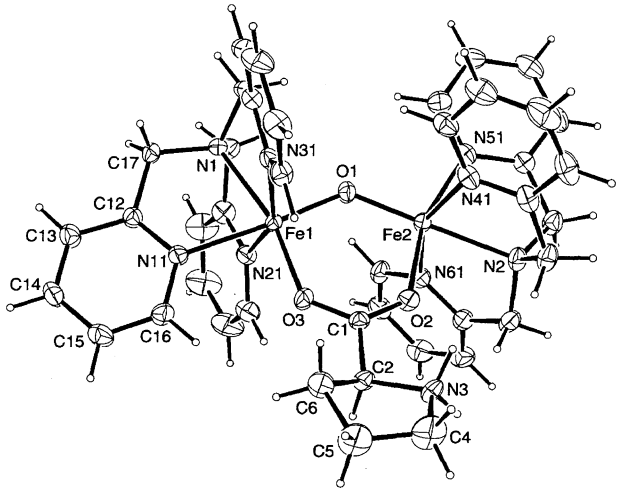

Fig. 2. ORTEP drawing of the complex cation in $[Fe_2(\mu\text{-}O)(\mu\text{-L-proline})(tpa)_2](ClO_4)_4 \cdot 2CH_3CN \cdot H_2O$ with the atomic numbering scheme showing 50% probability thermal ellipsoids.

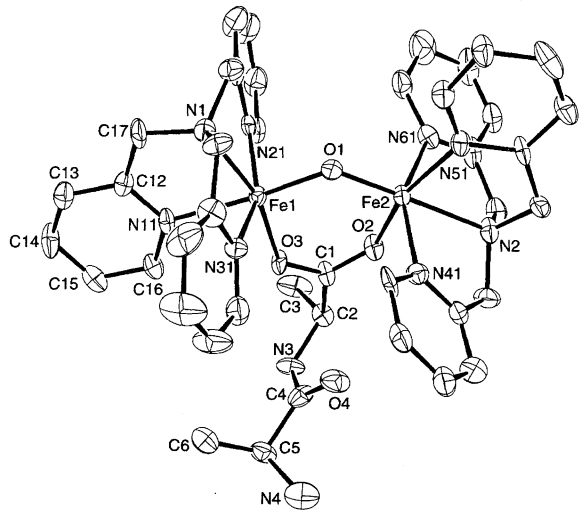

Fig. 3. ORTEP drawing of the complex cation in $[Fe_2(\mu\text{-}O)(\mu\text{-L-alanyl-L-alanine})(tpa)_2](ClO_4)_4 \cdot 2CH_3CN \cdot C_4H_9OH$ with the atomic numbering scheme showing 50% probability thermal ellipsoids.

Fe_2(III, III)(μ-O)(amH), are reduced. This process should be accompanied by the protonation to the oxo-bridge of the diiron complexes.[55,56] This is possible if the pK_a value of the oxide bridge at the Fe_2(II, III) state exceeds that of the zwitter ionic bridging amino acid. Proton-transfer may occur from the $-NH_3^+$ group of the amino acid either intramolecularly or intermolecularly from another nearby diiron complex ion. In either case, after the partial reduction, chemical species in equilibration would be the μ-hydroxo–Fe_2(II, III) with zwitter ionic amino acid, Fe_2(II, III)(μ-OH)(amH), and the μ-oxo-Fe_2(III, III) with deprotonated amino acid, Fe_2(III, III)(μ-O)-(am), since the amino group of the Fe_2(III, III) is expected to be more acidic than that of the Fe_2(II, III). Since the Fe_2(III, III)(μ-O)(am) species has less positive charge and higher electron density at the diiron center than the Fe_2(III, III)(μ-O)(amH), the former is reduced at more negative potential (E^2_{pc}) than the latter. However, a fully consistent interpretation of the observed redox behavior is difficult at the present stage, since we have not yet succeeded in isolating the reduced species by bulk electrolysis.

The proposed proton-coupled redox behavior of the diiron

Table 4. Correlation between the Difference of the First and the Second Reduction Peak Potentials (ΔE_{pc}) and Acid Dissociation Constants of Amino Acids in $[Fe_2(\mu\text{-O})(\mu\text{-amino acid})(tpa)_2](ClO_4)_4$

Amino acid	E^1_{pc}	E^2_{pc}	ΔE_{pc}	pK_1[a)]	pK_2[a)]
L-Proline (**2**)	+148	−63	211	1.90	10.38
L-Tyrosine (**4**)	+147	−59	206	2.17	9.04
L-Phenylalanine (**6**)	+147	−53	200	2.26	9.19
L-Tryptophan (**5**)	+135	−63	198	2.35	9.33
L-Alanine (**3**)	+101	−69	170	2.30	9.69
L-Valine (**1**)	+92	−64	156	2.26	9.49
L-Alanyl-L-alanine (**7**)	+40	−46	86	3.20	8.05

a) R. M. C. Dawson, D. C. Elliott, W. H. Elliott, K. M. Jones, "Data for Biochemical Research," 3rd ed, Oxford (1986).

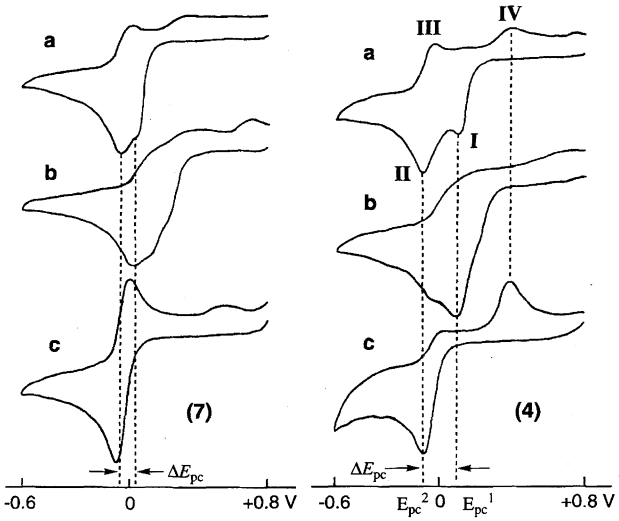

Fig. 4. Cyclic voltammograms of $[Fe_2(\mu\text{-O})(\mu\text{-amino acid})(tpa)_2](ClO_4)_4$ (amino acid = L-alanyl-L-alanine (**7**) and L-tyrosine (**4**)) in CH_3CN in the absence of acid nor base (**a**), in the presence of acid (**b**), and in the presence of base (**c**), where acid and base denote *p*-toluenesulfonic acid and triethylamine, respectively. Each dashed line shows the peak potential of the splitting reduction waves. The definition of the first (E^1_{pc}) and the second (E^2_{pc}) peak potential of the splitting reduction waves and the difference between the first and the second peak potentials (ΔE_{pc}) are also shown. **I**, **II**, **III**, and **IV** show the reduction wave of the original complex with zwitter ionic amino acid, the reduction wave of the complex with deprotonated amino acid bridge, the reoxidation wave of the μ-hydroxo diiron(II, III) complex with deprotonated amino acid bridge, and the reoxidation wave of the other structural core which is degraded from the μ-hydroxo diiron(II, III) core due to its instability, respectively.

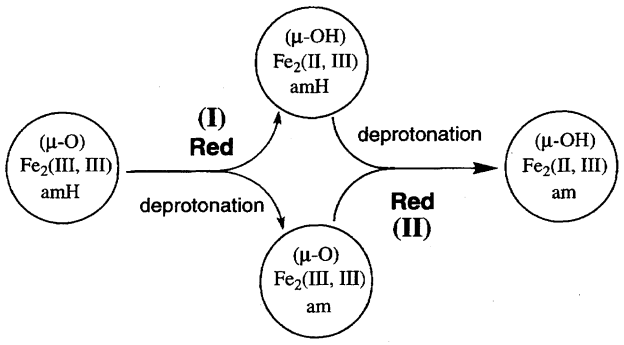

Scheme 1.

complexes may be supported by the similar redox behavior of the diruthenium complex $[Ru_2(\mu\text{-O})(\mu\text{-MeCO}_2)_2(bpy)(mim)_2]^{2+}$ (bpy = 2,2′-bipyridyl, mim = 1-methylimidazole) in acetonitrile.[57] The complex shows a reversible Ru_2(III, IV)/(III, III), quasi-reversible (III, III)/(II, III) and irreversible (II, III)/(II, II) processes in its cyclic voltammogram. The positive shift of the reduction potentials Ru_2(II, III)/(III, III) and Ru_2(II, II)/(II, III) was observed on addition of a strong acid, *p*-toluenesulfonic acid. The positive shift is accounted for by the protonation at the oxo-bridge at the Ru_2(II, III) and Ru_2(II, II) states. The pK_a values of the Ru_2(III, III) and the Ru_2(II, III) states have been estimated to be ca. 2 and 14, respectively. Thus a proton donor with the pK_a value smaller than 14 can transfer a proton to the oxo-bridge upon reduction from Ru_2(III, III) to Ru_2(II, III).

The reduction peak potentials (E^1_{pc} and E^2_{pc} values), their separation (ΔE_{pc}), and the acid dissociation constants (pK_1 and pK_2) of amino acids[58] are summarized in Table 4. The E^1_{pc} seems to have correlation with the pK_1 value, which indicates that the basicity of the carboxyl group of the zwitter ionic amino acid is important in determining the first reduction peak potential.[24] A similar trend was also observed for the oxo-centered trinuclear iron complexes.[47] Thus the negative shift of the first reduction peak potential is due to the decrease of the electron donation from the zwitter ionic amino acid bridge. However, there appears to be no clear trend between pK_2 values and either E^1_{pc} or E^2_{pc}. It is thus concluded that the deprotonation at the remote $-NH_3^+$ group would not give systematic electronic effect on the redox properties of the diiron redox center. Since the second reduction peak potential (E^2_{pc}) is almost invariant at around −0.06 V, ΔE_{pc} decreases with negative shift of the first reduction peak potential (E^1_{pc}).[59] The negative shift of the first reduction peak potential and therefore the decrease of ΔE_{pc} is parallel to the increase of the pK_1 value. Among the six complexes in Table 4, only the L-alanyl-L-alanine complex has $-NH_3^+$ group apart from the CO_2^- group by four atoms (only one atoms in the other complexes). Although the L-alanyl-L-alanine complex follows the general trend mentioned above, it is quite possible that its notably smaller ΔE_{pc} value may be related to the distance of the two functional groups. If the $-NH_3^+$ group is further apart from the CO_2^- group, we may not observe the splitting at all.

The authors are grateful to Prof. H. Oshio at Tohoku University for magnetic measurements. We are also grateful to Prof. A. Ichimura at Osaka City University and Prof. A. Odani at Nagoya University for valuable discussions. This work was supported by a Grant-in-Aid for Scientific Research No. 10133201 (Priority Area of "The Chemistry of Inter-element Linkage") to KU and No. 09237106 (Priority Area of "Electrochemistry of Ordered Interfaces") to YS from the Ministry of Education, Science, Sports and Culture.

References

1) R. G. Wilkins, *Chem. Soc. Rev.*, **1992**, 171.
2) K. K. Andersson, T. E. Elgren, L. Que, Jr., and J. D. Lipscomb, *J. Am. Chem. Soc.*, **114**, 8711 (1992).
3) R. E. Stenkamp, *Chem. Rev.*, **94**, 715 (1994).
4) K. E. Liu, A. M. Valentine, D. Wang, B. H. Huynh, D. E. Edmondson, A. Salifoglou, and S. J. Lippard, *J. Am. Chem. Soc.*, **117**, 10174 (1995).
5) B. E. Sturgeon, P. E. Doan, K. E. Liu, D. Burdi, W. H. Tong, J. M. Nocek, N. Gupta, J. Stubbe, D. M. Kurtz, Jr., S. J. Lippard, and B. M. Hoffman, *J. Am. Chem. Soc.*, **119**, 375 (1997).
6) S. C. Pulver, W. A. Froland, J. D. Lipscomb, and E. I. Solomon, *J. Am. Chem. Soc.*, **119**, 387 (1997).
7) L. Que, Jr., and A. E. True, *Prog. Inorg. Chem.*, **38**, 97 (1990).
8) K. Wieghardt, K. Pohl, and W. Gebert, *Angew. Chem., Int. Ed. Engl.*, **22**, 727 (1983).
9) S. Yan, L. Que, Jr., L. F. Taylor, and O. P. Anderson, *J. Am. Chem. Soc.*, **110**, 5222 (1988).
10) J. M. McCormick, R. C. Reem, and E. I. Solomon, *J. Am. Chem. Soc.*, **113**, 9066 (1991).
11) K. J. Oberhausen, J. F. Richardson, R. J. O'Brien, R. M. Buchanan, J. K. McCusker, R. J. Webb, and D. N. Hendrickson, *Inorg. Chem.*, **31**, 1123 (1992).
12) P. N. Turowski, W. H. Armstrong, S. Liu, S. N. Brown, and S. J. Lippard, *Inorg. Chem.*, **33**, 636 (1994).
13) Y. Zang, G. Pan, and L. Que, Jr., *J. Am. Chem. Soc.*, **116**, 3653 (1994).
14) Y. Zang, Y. Dong, L. Que, Jr., K. Kauffmann, and E. Münck, *J. Am. Chem. Soc.*, **117**, 1169 (1995).
15) Y. Dong, H. Fujii, M. P. Hendrich, R. A. Leising, G. Pan, C. R. Randall, E. C. Wilkinson, Y. Zang, L. Que, Jr., B. G. Fox, K. Kauffmann, and E. Münck, *J. Am. Chem. Soc.*, **117**, 2778 (1995).
16) M. Rapta, P. Kamaras, G. A. Brewer, and G. B. Jameson, *J. Am. Chem. Soc.*, **117**, 12865 (1995).
17) D. Coucouvanis, R. A. Reynolds, III, and W. R. Dunham, *J. Am. Chem. Soc.*, **117**, 7570 (1995).
18) A. Neves, M. A. de Brito, I. Vencato, V. Drago, K. Griesar, and W. Haase, *Inorg. Chem.*, **35**, 2360 (1996).
19) A. Ghosh, J. Almlöf, and L. Que, Jr., *Angew. Chem., Int. Ed. Engl.*, **35**, 770 (1996).
20) D. R. Gamelin, E. L. Bominaar, M. L. Kirk, K. Wieghardt, and E. I. Solomon, *J. Am. Chem. Soc.*, **118**, 8085 (1996).
21) L. Shu, J. C. Nesheim, K. Kauffmann, E. Münck, J. D. Lipscomb, and L. Que, Jr., *Science*, **275**, 515 (1997).
22) R. E. Norman, S. Yan, L. Que, Jr., G. Backes, J. Ling, J. Sanders-Loehr, J. H. Zhang, and C. J. O'Connor, *J. Am. Chem. Soc.*, **112**, 1554 (1990).
23) R. E. Norman, R. C. Holz, S. Ménage, C. J. O'Connor, J. H. Zhang, and L. Que, Jr., *Inorg. Chem.*, **29**, 4629 (1990).
24) R. C. Holz, T. E. Elgren, L. L. Pearce, J. H. Zhang, C. J. O'Connor, and L. Que, Jr., *Inorg. Chem.*, **32**, 5844 (1993).
25) Y.-M. Chiou and L. Que, Jr., *J. Am. Chem. Soc.*, **114**, 7567 (1992).
26) S. P. Watton, A. Masschelein, J. Rebek, Jr., and S. J. Lippard, *J. Am. Chem. Soc.*, **116**, 5196 (1994).
27) R. A. Leising, J. Kim, M. A. Pérez, and L. Que, Jr., *J. Am. Chem. Soc.*, **115**, 9524 (1993).
28) T. Kojima, R. A. Leising, S. Yan, and L. Que, Jr., *J. Am. Chem. Soc.*, **115**, 11328 (1993).
29) A. Hazell, K. B. Jensen, C. J. McKenzie, and H. Toftlund, *Inorg. Chem.*, **33**, 3127 (1994).
30) Y.-M. Chiou and L. Que, Jr., *Inorg. Chem.*, **34**, 3270 (1995).
31) J. Kim, R. G. Harrison, C. Kim, and L. Que, Jr., *J. Am. Chem. Soc.*, **118**, 4373 (1996).
32) W. B. Tolman, A. Bino, and S. J. Lippard, *J. Am. Chem. Soc.*, **111**, 8522 (1989).
33) Y. Dong, S. Ménage, B. A. Brennan, T. E. Elgren, H. G. Jang, L. L. Pearce, and L. Que, Jr., *J. Am. Chem. Soc.*, **115**, 1851 (1993).
34) N. Kitajima, N. Tamura, M. Tanaka, and Y. Moro-oka, *Inorg. Chem.*, **31**, 3342 (1992).
35) A. L. Feig and S. J. Lippard, *J. Am. Chem. Soc.*, **116**, 8410 (1994).
36) N. Kitajima, N. Tamura, H. Amagai, H. Fukui, Y. Moro-oka, Y. Mizutani, T. Kitagawa, R. Mathur, K. Heerwegh, C. A. Reed, C. R. Randall, L. Que, Jr., and K. Tatsumi, *J. Am. Chem. Soc.*, **116**, 9071 (1994).
37) A. L. Feig and S. J. Lippard, *Chem. Rev.*, **94**, 759 (1994).
38) B. J. Wallar and J. D. Lipscomb, *Chem. Rev.*, **96**, 2625 (1996).
39) L. Que, Jr., and Y. Dong, *Acc. Chem. Res.*, **29**, 190 (1996).
40) S. Herold and S. J. Lippard, *J. Am. Chem. Soc.*, **119**, 145 (1997).
41) A. L. Feig, A. Masschelein, A. Bakac, and S. J. Lippard, *J. Am. Chem. Soc.*, **119**, 334 (1997).
42) T. Ookubo, H. Sugimoto, T. Nagayama, H. Masuda, T. Sato, K. Tanaka, Y. Maeda, H. Okawa, Y. Hayashi, A. Uehara, and M. Suzuki, *J. Am. Chem. Soc.*, **118**, 701 (1996).
43) Y. Dong, S. Yan, V. G. Young, Jr., and L. Que, Jr., *Angew. Chem., Int. Ed. Engl.*, **35**, 618 (1996).
44) K. Kim and S. J. Lippard, *J. Am. Chem. Soc.*, **118**, 4914 (1996).
45) T. Tokii, K. Ide, M. Nakashima, and M. Koikawa, *Chem. Lett.*, **1994**, 441.
46) Y. Sasaki, K. Umakoshi, S. Kimura, C.-E. Oh, M. Yamasaki, and T. Shibahara, *Chem. Lett.*, **1994**, 1185.
47) K. Nakata, A. Nagasawa, Y. Sasaki, and T. Ito, *Chem. Lett.*, **1989**, 753.
48) W. F. Tucker, R. O. Asplund, and S. L. Holt, *Arch. Biochem. Biophys.*, **166**, 433 (1975).
49) R. C. Scarrow, M. J. Maroney, S. M. Palmer, L. Que, Jr., A. L. Roe, S. P. Salowe, and J. Stubbe, *J. Am. Chem. Soc.*, **109**, 7857 (1987).
50) G. Anderegg and F. Wenk, *Helv. Chim. Acta*, **50**, 2330 (1967).
51) A. Altomare, G. Cascarano, C. Giacovazzo, A. Guagliardi, M. C. Burla, G. Polidori, and M. Camalli, *J. Appl. Crystallogr.*, **27**, 435 (1994).
52) C. Edwards, C. J. Gilmore, S. Mackay, and N. Stewart, "CRYSTAN 6.3. A Computer Program for the Solution and Re-

finement of Crystal Structures," Mac Science, Yokohama, Japan (1995).

53) H. Yoshioka and K. Hirotsu, "BOND," Osaka City University, Osaka, Japan (1980).

54) On bulk electrolysis at −0.4 V, characteristic oxo-to-Fe(III) charge-transfer transition bands at ca. 490 nm and at 550—700 nm disappeared. The cyclic voltammograms of the electrolyzed solution of **4** and **7** show a quasi-reversible oxidation process (**IV/V**) at $E_{1/2}$ = +0.41 V (Fig. S1). On sweeping further toward negative direction, a small reduction peak corresponding to peak (**II**) is observed not accompanying with distinct peak (**I**). However, on bulk electrolysis (reoxidation) of the reduced solution at +0.7 V, the cyclic voltammogram and UV-vis spectrum of this solution coincided with those of the original solution before the electrolysis at −0.4 V. Multi-sweep cyclic voltammetry was also conducted for **1**—**7**. The first sweep shows the features as described above. Waves **I**, **II**, **III**, and **IV** for **4** appeared at +0.15, −0.06, +0.00, and +0.45 V, respectively. In the second sweep toward negative direction, the reoxidized species were reduced mainly at −0.06 V (wave **II**), though a new small peak (**V**) coupled with peak (**IV**) appeared at +0.37 V. These features are practically unchanged on further cyclic scans. The relative peak height of wave **V** and **I** depends significantly on the bridging amino acids. The complex **7** and **2** show no distinct peak (**V**), while these complexes show distinct wave **I**. The peak height of the redox couple (**IV/V**) increases and that of wave **I** decreases in the order of **7**, **2**, **3**, **5**, **6**, **1**, and **4**. The trend is similar to the increasing peak height of wave **IV** in the presence of triethylamine.

55) The pK_a value of the hydroxo-bridge of diiron(III) complexes, $[Fe_2(\mu\text{-}OH)(\mu\text{-}O_2CCH_3)(HBpz_3)_2](ClO_4)$ ($HBpz_3$ = hydrotris(1-pyrazolyl)borate, is estimated to be 3.5 (Ref. 12).

56) Our preliminary observation of the pH dependence of the redox potential Fe$_2$(III, III)/(II, III) by using self-assembled $[Fe_2(O)(\mu\text{-}SH(CH_2)_nCOO)(tpa)_2]^{3+}$ on Au electrode indicates that the pK_a of oxide bridge is < 3 at the Fe$_2$(III, III) state and > 10 at the Fe$_2$(II, III) state (T. Inomata, M. Abe, T. Kondo, K. Umakoshi, Y. Sasaki, and K. Uosaki, unpublished results).

57) A. Kikuchi, T. Fukumoto, K. Umakoshi, Y. Sasaki, and A. Ichimura, *J. Chem. Soc., Chem. Commun.*, **1995**, 2125.

58) A. E. Martell and R. M. Smith, "Critical Stability Constants," Plenum Press, New York (1974), Vol. 1.

59) After deprotonation, the bridging amino acid exists as a mono-anionic form. The average second reduction peak potential is about +0.16 V vs. NHE, which is close to the reduction potentials of $[Fe_2(\mu\text{-}O)(\mu\text{-}OAc)(tpa)_2](ClO_4)_3$ (+0.15 V)[24] and methemerythrin (+0.11 V),[60] though the effect of proton-transfer should be reflected on the reduction potential for amino acid-bridged complex.

60) F. A. Armstrong, P. C. Harrington, and R. G. Wilkins, *J. Inorg. Biochem.*, **18**, 83 (1983).